Viewing Classical and Relativistic Spacetime Geometry

D. V. Black* M. Gopi† F. Kuester‡ F. Wessel§ R. Pajarola¶

University of California at Irvine

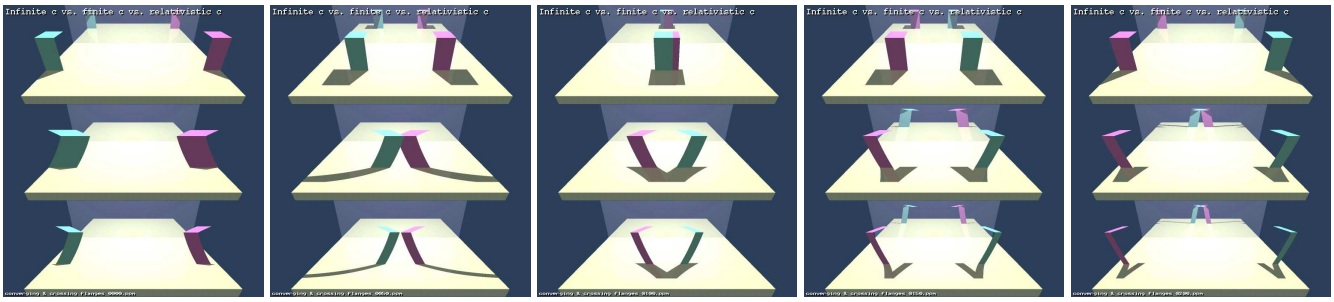

Figure 1: 4D objects converging then crossing at 0.866 c on a mirrored background
Top: traditional raytracing; Center: classical spacetime model; Bottom: relativistic spacetime model

Abstract

Recent advances in physics have suggested new models that incorporate multiple spatial dimensions to explain new cosmological evidence. These new theories are a challenge to envision and difficult to grasp. Adapting visualization algorithms and strategies to the new physics of multiple dimensions can aid in understanding these non-intuitive phenomena.

This paper presents an adaptation of 4D ray tracing to a spacetime model that captures Einstein's geometry and shows how relativistic phenomena such as Terrell rotation, aberration, retarded time and even animation and motion blur, can emerge from a static spacetime model. This technique has made it possible to explore the fundamental nature of Einstein's geometric model by decoupling finite light-speed from time dilation and length contraction. The simplicity of the model also suggests new pedagogical techniques that may invigorate physics education.

CR Categories: I.3.5 [Computer Graphics]: Computational Geometry; Temporal Extrusion— [I.3.7]: Computer Graphics—Animation; 4D Raytracing J.2 [Physical Sciences and Engineering]: scientific visualization; relativistic effects; temporal extrusion— [K.3]: Computers and Education—educational technology

Keywords: raytracing, spacetime, relativity, Einstein, 4D, animation, visualization

*The Graphics Group; Computer Science, UCI; e-mail:dblack@ieee.org
†The Graphics Group; Computer Science, UCI; e-mail:gopi@uci.edu
‡Calit2 Center of GRAVITY, UCI; e-mail:fkuester@uci.edu
§Physics & Astronomy, UCI; e-mail:fwessel@uci.edu
¶Visualization and Multimedia Lab, University of Zürich; e-mail:pajarola@acm.org

1 Introduction

With the advent of the workstation, the visualization of non-intuitive physical phenomena such as objects in 4D space and 4D spacetime has become a reality. Since the 1980's, papers, images, and animations have appeared demonstrating that these phenomena no longer need be relegated to the domain of the esoteric researcher. Rather, the contemporary student of physics with the aid of the ubiquitous visual computer, can have a hands-on experience with these phenomena.

The challenge is to go beyond visualization of special relativity or spacetime. This paper provides a method for visually conceptualizing higher dimensions. The strategy is demonstrated using 4D spacetime (3 spatial + 1 temporal dimensions), a dimensionality that has been visited in the computer graphics literature. Since it is possible to conceptualize spacetime viewing by extrapolating from 3D viewing, it may also be possible to view higher dimensions by a similar process.

In our approach, time is treated as a fourth geometric dimension with certain constraints described below. The results of viewing this higher dimensional spacetime are compared to the results of contemporary special relativistic visualization. If our strategy yields similar results, it should be possible to create a simple yet accurate model for a geometric interpretation of Einstein's spacetime and a pedagogy to explain the phenomena. For simplicity, we assume that spacetime is flat (there is no mass), there is no acceleration, and the camera is at rest in the laboratory's inertial reference frame (the camera frame). The single light source is also at rest in the camera frame.

Our geometric model treats 3D objects as cross-sections of 4D objects projected into 3-space. The 4-space is probed via photon paths which lie on the surface of a right circular hypercone, known as the ***lightcone***. The lightcone's symmetrical axis is collinear with the negative time ($-t$) axis. This results in a cross section of 4-space that corresponds to the intersection of the lightcone's surface with embedded 3-manifolds. The resulting visualization of this projection should have the same properties as those provided by contemporary relativistic visualization tools.

The 3+1 dimensional approach was selected to adhere to Einstein's geometric vision of light propagation [6]. Representing 3D objects in spacetime and ray tracing 3D manifolds in 4D is ex-

plained in detail beginning with a brief overview of the theory, then presenting the simple geometric algorithms and their implementation.

1.1 Background

For a definitive treatment of Einstein's Theory of Special Relativity, the reader is directed to the physics literature [6][14][3][19] .

This paper will visually explore two phenomena of spacetime: the visual effects of finite lightspeed; and the physical effects of Special Relativity. The former visual only effects[1]which are due to the delayed light signal are referred to as ***classical***, while the latter physical effects are referred to as ***relativistic***. There is an interesting relationship between the ***classical*** and ***relativistic*** phenomena as pointed out by Terrell [21], Penrose [17] and Boas [2]: in that the two effects can cancel each other out in some cases.

The *classical* effects of finite lightspeed are simply the apparent distortions to an object that are the result of light from portions of the object at different distances from the observer arriving at different times. A rapidly moving object's physical shape can be determined simply by compensating for the delay introduced by the finite speed of light.

Relativistic effects result from Einstein's relativity, and are real and physical, not merely apparent. Einstein's two postulates of special relativity are:

1. **The Relativity Postulate:** The laws of physics are the same for observers in all inertial frames. No one frame is a preferred frame.
2. **The Speed of Light Postulate:** The speed of light in vacuum has the same value (c) in all directions and in all inertial frames.

In the relativistic model, any observer traveling at any velocity will measure the speed-of-light in a vacuum to be approximately 3×10^8 m/s. In a 3D space, these principles require both length-contraction and time-dilation for consistency with observed phenomena [7]. That is to say, two different observers traveling at different velocities will measure the other observer's meter-stick as shorter and the other observer's clock as slower than their own.

This paper will graphically demonstrate that a geometric model can be created wherein 3D objects are considered to be cross sections of 4D objects projected into 3-space, and that the 4D objects can be treated as rigid, assuming that there is negligible mass. A method is provided to convert a given 3D object into a 4D spacetime object, and to observe the converted objects from the camera's inertial reference frame. This geometric implementation will be shown to yield results equivalent to those of prior non-geometric visualizations.

1.2 Related Work

Various algorithms and techniques have been developed by physicists, scientists and educators for visualizing relativistic effects in Minkowski 4D spacetime [10][11][20][18]. The two predominate approaches are polygonal rendering and ray tracing.

1.2.1 Polygonal Rendering

In Euclidean 4-space, the polygon rendering approach is implemented by extending the algorithms of 3D object projection to 4D objects in order to project these 4D objects onto a conventional 2D imageplane [4]. Since special relativistic visualization occurs properly within the context of a non-Euclidean 4D spacetime, the approach for visualizing 4D spacetime is subtly different from that for a Euclidean 4-space. While not necessary for the Euclidean 4-space approach, a Lorentz transform[2]is necessary in the non-Euclidean 4-space to convert from the object's inertial reference frame to the inertial reference frame that contains the imageplane (the camera frame).

Hsiung, Thibadeau, and Wu [13] implemented such a strategy in 1990 with their novel time-buffer approach, which used graphic Z-Buffer hardware to optimize performance. The time-buffer algorithm performed conventional 3D rendering in the object's rest frame, and then performed a Lorentz transform operation on each of the pixels in the object's imageplane to convert to the camera's imageplane. The time-buffer then filtered for the most recent ray-object intersection event for each pixel.

Rau, Weiskopf, and Ruder [18] implemented a polygon renderer in 1997 in which the 3D objects in the object frame were Lorentz transformed into 3D *photosurface* objects in the camera frame. The new *photosurface* object, which approximated the shape of the object as viewed from the camera frame, was then projected onto the camera's viewplane using conventional 3D rendering techniques.

1.2.2 Ray Tracing

In 1988 Glassner [10] developed an optimization strategy exploiting temporal coherence for conventional 3D raytracing. In his approach, 3D objects were raytraced in 4D space, resulting in up to 50% processing time improvement. He also demonstrated that motion blur could be generated by varying the camera's time component. Although he did not demonstrate relativistic visualization with his algorithm, he did suggest it as a direction for future research.

In 1989 Hsiung and Dunn, developed a relativistic ray tracing algorithm. In their implementation, 3D objects were imported and maintained in their own inertial reference frame in which they are at rest. Each conventionally traced 3D ray is *Lorentz-transformed* from the camera frame to each of the objects' frames and the usual 3D ray tracing intersection occurs in the object's rest frame, with the most recent intersection selected. Color information is interpreted and *Lorentz-inverse-transformed* back to the camera frame for display. Reflecting rays are likewise *Lorentz-transformed* from their originating frame to another object or light-source frame for intersection determination, and their color information *Lorentz-inverse-transformed* back to the reflecting frame. A technique for color power spectrum processing via B-spline interpolation was implemented by Hsiung, et. al. in 1990 [12].

In 2001, a promising approach was introduced by Weiskopf in his PhD Dissertation [23] in which he described and built a four dimensional General Relativity ray tracer. This model supported only geometric effects, and secondary rays and shadow rays were neglected.

1.2.3 Other Methods

In 2000, Weiskopf introduced an interesting special relativistic visualization method using image based rendering [22]. The strategy was implemented by applying relativistic aberration to each pixel of the visual sphere surrounding the observer, thus warping the geometry of observed objects. If a wavelength-dependent plenoptic function is provided with sufficient bandwidth, then the transformed pixel's power-spectrum can be generated from the untransformed image. The algorithm can be adapted to texture mapping hardware for real-time performance with data acquired by standard cameras.

Weiskopf's 2001 dissertation [23] provides a comprehensive description of relativistic visualization technologies and their history.

[1]Sometimes referred to as Galilean relativity or Newtonian relativity. The Galilean transform assumes that the geometry of space is Euclidean.

[2]"the Lorentz transform corresponds to a 'rotation' of the co-ordinate system in the four-dimensional 'world'" - Einstein [8].

1.3 Our Approach

The techniques used to visualize special relativity typically use 3D raytracing of 3D objects, with additional logic to handle the velocity matching and Lorentz transforms, operations that are not required with 3D visualization. It would be advantageous if an algorithm could be found for which no special logic and transforms are required to simulate the geometry of relativistically moving objects. A suitable algorithm would reduce the special cases and associated logic to less than that required with 3D visualization.

Traditional 3D animation simulates the motion of objects by repositioning the objects in the scene between frames. In our method described here, the 4D objects are static, and only the camera's temporal position is changed between frames. The novelty of this model is its adherence to a geometric interpretation of Einstein's spacetime concepts[3]. The postulates and fundamental principles of relativity are used as the basis for these techniques. Ray tracing of 4D spacetime was selected as the best technology due to its conformity to a more natural interpretation of Einstein's spacetime. This paper also introduces ***temporal extrusion***, a simple operation to extend a 3D object into 4D spacetime. For simplicity, this paper will emphasize the visualization of the geometry of objects with constant velocities. Although not demonstrated here, the concepts can be generalized to accelerating objects with curved 4D paths via curved temporal extrusions.

2 THEORY

2.1 Special Relativity Terminology

Einstein's 4D spacetime (t,x,y,z) model consisting of both space and time, is often referred to as (3+1)D, that is, three isotropic spatial dimensions (x,y,z) and one anisotropic time dimension (t). This convention will be used throughout this paper.

A 4D spacetime point (t,x,y,z) will be referred to as an ***event***.

It is assumed that spacetime is flat - there is negligible mass. The path of a lightray is therefore a straight line, as is the path of an object with a constant velocity.

The camera will lie on the t axis, thus its spatial components will always be zeros: $(t,0,0,0)$. The terms camera and point-of-view (POV) may be used interchangeably. (Purists may wish to conceptualize a pin-hole camera that does *not* invert the image, with the pin-hole at the POV [10].)

For this discussion the camera frame's 3D axes will be rotated such that the x axis is parallel with the object's velocity vector, so $\Delta z = \Delta y = 0$. Speed will be measured as a fraction ($\beta = \frac{v}{c}$) of lightspeed (c).

The ***worldline*** of an object marks the object's path through 4-space from event to event. An object whose worldline is parallel to the camera's t (time) axis is stationary in the camera frame, since there is no Δx, hence $V = \frac{\Delta x}{\Delta t} = 0$

An object whose worldline that is not parallel to the t axis has a velocity, since $\Delta x \neq 0$.

The instantaneous tangent of the worldline of an object is the object's velocity 4-vector (τ) in the camera frame. In the object's rest frame, this velocity vector is also the ***proper*** time (t) axis for the **inertial reference frame** in which the object is at rest (the object frame). For an object with a constant velocity (no acceleration) in an inertial reference frame, the worldline and the velocity 4-vector for that object are identical. The velocity of an object in the camera frame is a monotonically increasing function with respect to the angle between the object's velocity 4-vector (worldline) and the time axis of the camera frame.

[3]"... the four-dimensional space-time continuum of the theory of relativity, in its most essential formal properties, shows a pronounced relationship to the three-dimensional continuum of Euclidean geometrical space." - Einstein [9]

Temporal extrusion is the construction of a higher-order (n-D) object by extruding its lower-order ($(n-1)$-D) counter part along its velocity 4-vector, and connecting its respective bounding $(n-2)$-D simplices to create $(n-1)$-D simplices bounding the higher-order object. For example, a prism could be created by extruding a triangle parallel to the triangles's t axis.

The operation optionally includes applying a Lorentz transform to objects whose extrusion angles are not parallel to the camera (laboratory) frame's time axis. A ***Lorentz-decoupled*** (or classical) object is one which was inserted into the scene without the Lorentz transform (an un-physical object).

Planck or natural units, which are unitless ($c = 1$), will be used throughout this paper for convenience. The benefit of natural units is that the units of measure along all the spacetime axes are similar, i.e. the t axis as well as the $x,y,\&z$ axis have the same scale and identical units of measure.

This is equivalent to stating that the t axis has been scaled by c (speed-of-light), yielding a ct axis. A lightray will travel one unit (of Euclidean distance) along the spatial axes for each unit it travels along the time axis - the lightrays always bisect the angle between the time axis and the 3 spatial axes. In other words, the 't' component of the normalized lightray direction 4-vector shall always be $-\frac{\sqrt{2}}{2}$. Furthermore, the lightrays lie on the hypersurface of a bisecting hypercone (depicted in Figure 5) whose apex is at the origin and whose symmetric axis is collinear with the negative time axis. In other words, the traced rays always lie at 45° to the $-t$ axis.

By convention, the term ***relativistic velocity*** will be used to describe speeds between the two referents of approximately 0.866 of lightspeed ($0.866c$) or greater. In some cases the term ***relativistic*** is used as a modifier to describe an object that is moving with relativistic velocity with respect to the camera frame or a referent observer.

2.2 Expectations

Special Relativity theory makes certain predictions about what can be expected in viewing a relativistically moving object. But, as implied in Section 1.1, it is important to not confuse relativistic effects with classical effects. The relativistic effects are length-contraction and time-dilation. Among the classical effects are retarded time, aberration, and Terrell rotation. These classical effects are also affected by special relativity, which makes them difficult to observe empirically. However, a suitable model will allow both the classical and relativistic components of these phenomena to be visualized both separately and together.

2.2.1 Classical Retarded Time

The term ***retarded time*** refers to the delay in the arrival of information about an event due to the distance of an event and the finite speed-of-light. For an observer and an event in the same inertial reference frame, the soonest that the light from an event 10 light-seconds away can reach the observer is 10 seconds after the event has occurred.

As an example, consider the case of a fast high flying jet. The point of origin of the sound seems to trail the jet across the sky due to the finite speed of sound. This effect is merely apparent (a classical effect), not physical (not a relativistic effect). The jet's true position can be measured simply by compensating for the time delay introduced due to the finite speed-of-sound.

Likewise, the appearance of an object is communicated causally to an observer from the spacetime positions of the object at some points in the past. The times that the light left each of the object's surface elements could be different since the object's elements are most likely at different distances from the observer. This will result in a visual distortion of the geometry of the object, if the object is

moving with respect to the observer. The greater the velocity, the more apparent the distortion.

The following apparent geometric distortions are visual effects resulting from the aforementioned retarded time phenomena which is an effect of finite lightspeed. The classical effects to be discussed here are non-relativistic aberration, and the non-relativistic component of Terrell rotation. The magnitude of these effects can be affected by Special Relativity.

2.2.2 Classical Aberration

Aberration is a deflection in the distribution of stars in the celestial sphere towards the direction of the motion of the Earth through space. Relativistic aberration is a distortion in the visual sphere about an observer moving through a scene with a relativistic velocity. Non-relativistic aberration is the classical component of aberration that is independent of relativity. As the velocity of the observer increases, the objects in the scene slide towards the front of the observer's sphere of vision. That is, the angle between the observer's velocity vector and the angle of incidence of the light ray from an observed object decreases monotonically as the velocity increases such that the light from the object seems to come from a position closer to the front of the observer. Due to the nature of relativity (the First Postulate), the evaluation gives the same results if the object and observer are exchanged such that the observer is at rest and the object is passing the observer with a relativistic velocity.

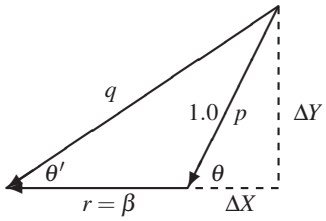

Figure 2: Classical Aberration

As shown in Figure 2, classical aberration is the apparent angle (θ') of a moving object, which can be determined from simple 3D vector subtraction of the observer's velocity vector (r) from the lightray's velocity vector (p). From the figure, it can be seen that $\tan\theta' = \frac{\Delta Y}{\Delta X + r}$. Scaling the figure so that $p = 1.0$ sets $\Delta Y = \sin\theta$ and $\Delta X = \cos\theta$. This yields the following equation where β is the velocity of the object towards the observer ($\beta = \frac{v}{c}$), θ is the angle of incidence of the lightray to the observer, and θ' is the apparent angle of the lightray to the observer:

$$\tan\theta' = \frac{\sin\theta}{\cos\theta + \beta} \tag{1}$$

As can be seen from the equation, the apparent angle of incidence (θ') of the lightray from the source to the observer will decrease monotonically with respect to the at-rest angle (θ) as the velocity (β) increases.

2.2.3 Relativistic Aberration

Relativistic aberration is the deviation of the apparent angle of a relativistic object from the angle to the object with respect to an observer. This analysis requires the introduction of the Lorentz factor, γ, where $\beta = \frac{v}{c}$, as defined above:

$$\gamma = \frac{1}{\sqrt{1-\beta^2}} \tag{2}$$

The relativistic aberration can be determined from the following equations where α replaces θ as the angle of incidence of the lightray to the observer, and α' replaces θ' as the apparent angle of the lightray to the observer:

$$\cos\alpha' = \frac{\cos\alpha + \beta}{1 + \beta\cos\alpha} \tag{3}$$

$$\sin\alpha' = \frac{\sin\alpha}{\gamma(1 + \beta\cos\alpha)}) \tag{4}$$

$$\tan\alpha' = \frac{\sin\alpha'}{\cos\alpha'} = \frac{1}{\gamma}\frac{\sin\alpha}{(\cos\alpha + \beta)} \tag{5}$$

Equation 3 was published by Einstein in 1905 [5]. Equation 4's derivation is shown by Rindler [19]. When Equation 5, as shown by Pauli [16], is compared to Equation 1, the analytic difference between the classical and relativistic effects can be shown to be a function of Lorentz length contraction:

$$\tan\theta' = \frac{\sin\theta}{\cos\theta + \beta} \tag{6}$$

$$\tan\alpha' = \frac{1}{\gamma}\frac{\sin\theta}{\cos\theta + \beta} \tag{7}$$

$$\tan\alpha' = \frac{1}{\gamma}\tan\theta' \tag{8}$$

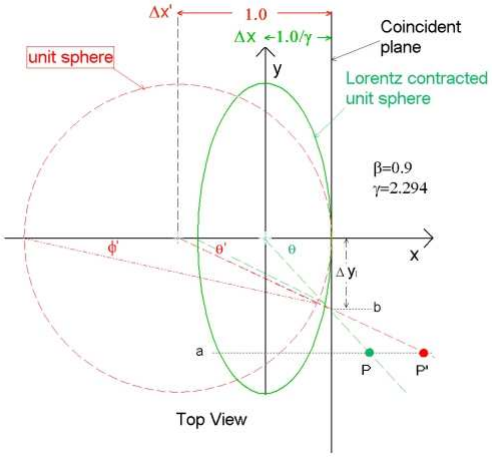

Figure 3: Relativistic aberration

A physical interpretation of the Lorentz factor is shown in Figure 3 and described as follows. The visual sphere of the observer G in frame *Green*, which G perceives as spherical, appears oblate with respect to the rest frame. The lightray intersects G's visual sphere at angle of incidence, θ where $\tan\theta = \frac{\gamma\Delta Y}{\Delta X}$. However, since G sees frame *Green* as at rest and spherical, as depicted by the dashed circle (frame *Red*), G determines the angle of incidence to be $\tan\theta' = \frac{\Delta Y}{\Delta X}$. Consequently, G in frame *Green* perceives the angle of incidence of the lightray to be less than that seen by an observer at rest.

While Equation 8 shows an elegant analytical relationship between classical and relativistic aberration, it has a singularity at 90 degrees. Terrell [21] solved this problem by using the trigonometric half-angle formula to derive the following relativistic aberration equation:

$$\tan\frac{\alpha'}{2} = \sqrt{\frac{(1-\beta)}{(1+\beta)}}\tan\frac{\alpha}{2} \tag{9}$$

As with the classic Equation 1 and the relativistic Equation 8, the apparent angle of incidence ($\theta'\&\alpha'$) of the lightray from the source to the observer will decrease monotonically with respect to the incoming angle (θ) as the velocity (β) increases. Multiplying Equation 9 by $\frac{(1+\beta)}{(1+\beta)}$ yields a more intuitive representation as can be seen from the geometry of Figure 3 where the visual sphere is length-contracted by $\frac{1}{\gamma}$:

$$\tan\frac{\alpha'}{2} = \frac{1}{\gamma}\frac{\tan\frac{\alpha}{2}}{(1+\beta)} \tag{10}$$

Figure 15 is included in the Results Section 4 to visualize this relativistic aberration.

2.2.4 Terrell Rotation

The optical effect known as Terrell rotation can be attributed to a combination of classical effects and relativistic effects: specifically retarded time and relativistic aberration. Since the backside of an object (the side facing away from the camera) is further from the camera than the frontside (the side facing the camera), the light from the backside will be delayed. Depending on the shape and velocity of the object, it is possible for the object to dodge its own lightray emanating from an obscured portion of the object. The backside or distant portions of an object moving relativistically past an observer, would appear to trail after the object (as if it were blowing in the wind). This phenomena causes the object to appear rotated to face in the direction of its motion, and is known as Terrell rotation.

Although a classical effect by our definition, Boas [2] predicted that relativistic straight lines would appear curved to an observer. Terrell [21] predicted that in certain cases the length-contraction can be masked by the classical (Terrell) rotation.

3 Algorithms

In order to visualize both the classical and relativistic effects described in Section 2.2, a modified raytracing mechanism was chosen to represent the geometric model described by Einstein[4]. The presented variant of raytracing, unlike conventional raytracing implementations, takes into account the finite speed of light.

A conventional raytracing engine determines the color of a pixel by passing a lightray from the camera through each pixel of the image plane and out into the 3D scene. If the lightray intersects an object, then the color of the object, modified by a suitable color model, is transferred to the pixel of the image plane. The algorithm is more complex when the lightray has a finite velocity.

In order to find the intersection of a finite speed lightray with 3D objects, the model must account for the changing positions of moving 3D objects as the lightray travels towards the camera. For multiple intersections the model must find the object-intersection closest to the camera. Furthermore, the model must account for length-contraction and time-dilation.

From the Principles of Special Relativity as delineated in Sections 1.1 and 2.1, the following set of specifications was formalized.

1. All objects in the scene will be instantiated in a common laboratory inertial reference frame. The camera and light source, both at rest, will be instantiated in the laboratory frame.
2. A 4D object is created from a 3D object by ***temporal extrusion***, that is extruding the object along its velocity 4-vector in the laboratory frame:
   (a) The velocity of the extruded object is the extrusion's spatial change divided by the temporal change;
   (b) If an object's extrusion vector (worldline) is parallel to the camera's t axis, then the object appears to be static; otherwise it appears to be moving;
   (c) The Lorentz transform (LT) is determined from the object's extrusion vector's spatial to temporal ratio ($\frac{\Delta x}{\Delta t}$) as follows:
      i. $\beta = \frac{\Delta x}{\Delta ct} = \frac{\Delta x}{\Delta t} \times \frac{1}{c}$
      ii. $\theta = \operatorname{arctanh}\beta$
      iii. $$LT = \begin{bmatrix} \cosh\theta & -\sinh\theta & 0 & 0 \\ -\sinh\theta & \cosh\theta & 0 & 0 \\ 0 & 0 & 1 & 0 \\ 0 & 0 & 0 & 1 \end{bmatrix}$$
   (d) The Lorentz transform is applied to the object prior to the object's insinuation into the laboratory frame (except *Lorentz-decoupled* objects). Length-contraction modifies the object geometry, and time-dilation modifies time dependent aspects of the object such as its color and lifetime.
3. Lightrays will be constrained to lie on the hypersurface of a right circular hypercone symmetric about the t axis thus yielding a constant lightspeed ($c = 1.0$) in natural units. This hypersurface bisects the angle between the negative time axis and the spatial axes.
4. For each video-frame, an image will be generated by iteratively passing a ray from the camera's POV through each pixel in the imageplane (or visual sphere about the POV) such that the ray lies on the hyperconical surface, and out into 4-space where it may intersect with a 3-manifold defining a 4D object in the 4-space. For multiple intersections, the intersection closest to the camera (most recent) is selected.
5. For each video-frame, imageplane pixels will be colored by extracting the 3D properties of the Lorentz transformed 4D object at the point of lightray/object intersection. It shall be assumed that the light source is at rest in the laboratory (camera) frame, and that the contributions of the moving objects to one another's local diffuse lighting are trivial (and does not contribute to the objects' geometry).
6. Advancing the camera along the t axis is equivalent to advancing the scene ahead in time. A sequence of animated views will be generated by incrementing only the t component of the camera's (and viewplane's) 4D position for each video-frame with no modification to the objects in the worldspace.

3.1 Object Construction

A 3D object can be visualized by rendering the 2D faces connecting its 1D edges. The 4D objects shown here are visualized by rendering the 3D hyper-faces connecting their 2D faces (Figure 4).

Extrusion is a common 3D Computer Aided Design (CAD) operation whereby a 2D object is transformed into a 3D object by extruding the object along a vector perpendicular to the plane in which the 2D object lies. Likewise, the extrusion of a 3D object into 4-space is accomplished by extruding the object along a vector perpendicular to the hyperplane (3-space) in which the object lies.

Temporal extrusion is a similar spacetime operation. A 3D object is extruded along a vector perpendicular to the hyperplane in which the object lies. That perpendicular is the *object*'s proper time axis (*not* the camera's time axis). Since the object's velocity vector

[4]"Formally, these four co-ordinates correspond exactly to the three space co-ordinates in Euclidean geometry" - Einstein [9]

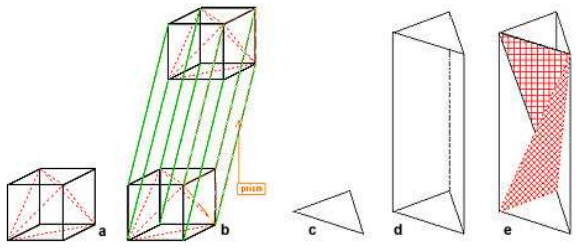

Figure 4: Cube & Triangle: Extruded then tessellated

is also the object's time axis in this model, the object is actually extruded along the velocity 4-vector.

As with conventional 3D rendering, complex objects are constructed from simple primitives. In this case, the primitives are 2D triangles in 3D space extruded along their common time axis into 4D. For example, each of the 12 triangles of the cube in Figure 4a is extruded parallel to its time axis for a distance equivalent to the time the cube is in existence (and at a constant velocity) thus creating a 3D hypersurface (or 3-manifold) in 4-space (Figure 4b).

Any 3D object defined by bounding triangles (Figure 4) can be ***temporally extruded*** into a 4D hyperobject and inserted in the scene's 4-space (the model database) as follows. First insert a t component into each of the vertex coordinates and set t to some constant value, say t_0:

$$(x_i, y_i, z_i) \rightarrow (t_0, x_i, y_i, z_i).$$

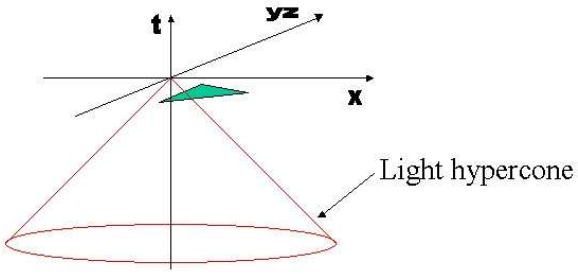

Figure 5: 2D face prior to temporal extrusion

The object now lies embedded in the t_0 hyperplane orthogonal to the t axis (Figure 5). In other words, the object instantly appears for a moment at $t = t_0$. Each of these triangles, and hence the object composed from them, can be extruded into the 4th dimension by duplicating the vertices of the triangle with lessor (or greater) values for the t components. If the object is at rest in the camera frame, a constant, Δt, can be added to the t components, before each triangle is extruded from the original (t_0) hypersurface to the new duplicate ($t_0 + \Delta t$) hypersurface. As in Figure 6 where $\Delta t < 0$, connecting the respective vertices of the extruded and original triangle pairs creates a prism from each triangle:

$$(x_i, y_i, z_i) \rightarrow (t_0, x_i, y_i, z_i) + (\Delta t, \Delta x_i, \Delta y_i, \Delta z_i) \rightarrow (t_1, x_i, y_i, z_i)$$
$$where \;\; \Delta x_i = \Delta y_i = \Delta z_i = 0 \rightarrow v = 0$$

The prisms are then tessellated into three adjacent tetrahedra simply by using a table to connect two triads of vertices by way of two triangles as shown in Figure 4. The 3D simplices are necessary for the Barycentric algorithm used to find precisely where, *on* the 3-manifold (i.e. *within* the 3D hyper-face) of the 4D object the intersection with the ray occurs.

An object's velocity is represented by changing the position of the extruded end of the triangle (Figure 7) with respect to the original end, e.g. $x_{end} = x_{beg} + 2.0$, so that $\Delta x = 2.0$ spatial units. The speed would thus be 2.0 $\frac{spatial\ units}{time\ unit}$.

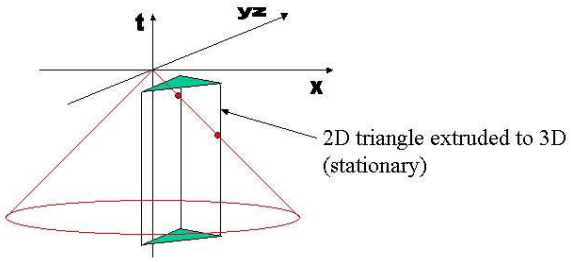

Figure 6: Triangle at rest extruded through lightcone

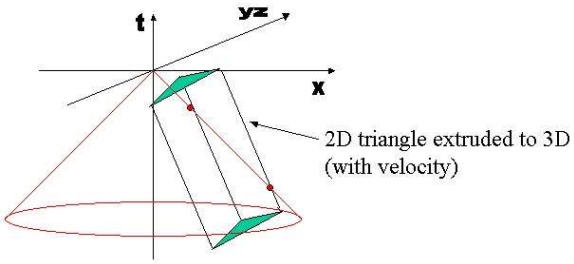

Figure 7: Temporal extrusion not parallel to 't' axis

Two classes of 3D objects have been implemented in the software: the Hyper-object (H_{obj}) and the Virtual-object (V_{obj}). Conceptually, the H_{obj} is observed passing through the laboratory inertial reference frame at a relativistic velocity, and so the measurements of the object are already in the laboratory's subjective units, meaning it is already length-contracted and time-dilated. This H_{obj} is added to the database using its subjective dimensions as seen in the camera frame, since it is already Lorentz transformed. This H_{obj} class is used to specify *Lorentz-decoupled* objects.

The V_{obj} is likewise passing through the lab frame at a relativistic velocity, but has been observed at rest, and the object size is obtained from its own rest frame. The V_{obj} is entered into the database using its proper rest dimensions, and a velocity vector in the laboratory (camera) frame. The virtual object must thus be Lorentz transformed from its rest frame to the laboratory frame as it is instantiated in the scene. The velocity 4-vector $(\Delta t, \Delta x, \Delta y, \Delta z)$ contains the numeric lifetime of the object as the temporal (Δt) component, and the travel distance in time Δt as the spatial $(\Delta x, \Delta y, \Delta z)$ components.

If an object's extrusion vector is kept to less than 45° with respect to the t axis (i.e. inside the lightcone), then it will have a velocity less than that of light. As an interesting aside and an extension to the standard model, super-luminal velocities may be represented via (Lorentz-decoupled) objects with extrusion angles greater than 45°.

3.2 Viewing 3D Objects in (3+1)D Spacetime

Consider a 3D viewfrustum in 3-space (x, y, z), whose camera lies at the origin, and whose line-of-sight is collinear with the x axis. If a 3D object such as a cube were placed within the 3-space viewfrustum, the object can be viewed via traditional raytracing.

Figure 8 depicts a hypercone in 4-space (t, x, y, z), whose symmetric axis is collinear with the $-t$ axis, and whose apex is coincident with the origin $(0, 0, 0, 0)$. This hypercone's hypersurface has 3 dimensions, sufficient to contain the 3D viewfrustum. Although it is a 3-manifold in 4-space, this hypercone is known as a ***lightcone***.

Conceptually, to account for the finite speed of light, the viewplane can be considered to be spherical thus allowing lightrays from

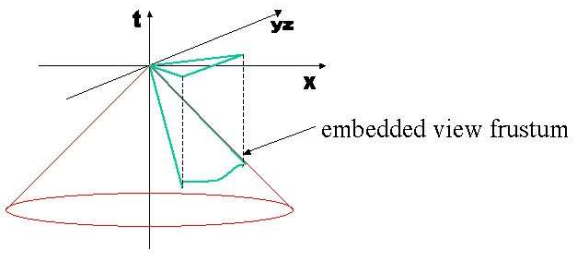

Figure 8: Viewfrustum projected onto lightcone

all pixels to reach the view point at the same time, and so do not contribute to geometric distortion. This viewplane is extruded along the negative time axis and is guaranteed to remain on the light cone. Such an extrusion is shown in Figure 8. Since it is a right circular hypercone, the 4D camera coordinate is (0, 0, 0, 0), while the viewplane coordinates for each pixel (p) are:

$$(t_p, x_p, y_p, z_p) = (-\sqrt{x_p^2 + y_p^2 + z_p^2}, x_p, y_p, z_p) \quad (11)$$

As depicted by the red or shaded dots in Figures 6 & 7, a camera located at the origin of this 4D model can see only those 3D objects whose extruded tetrahedra intersect the lightcone, that is vertex extrusion pairs (t_0, x_i, y_i, z_i) & (t_1, x_i, y_i, z_i), where:

$$t_0 >= ||(x_i, y_i, z_i)|| >= t_1, \forall \ \{(t_0, x_i, y_i, z_i) \ \& \ (t_1, x_i, y_i, z_i)\} \quad (12)$$

Lightcone crossing events are detected by solving for the intersection of a lightray with each of the bounding tetrahedra. The set of lightrays is defined as that set of 4D straight lines passing from the camera through each of the pixels in the viewplane's pixel grid and out into 4D space. Using a barycentric algorithm the intersections of the ray with all tetrahedra faces are determined, and that intersecting event nearest to the camera (i.e the t value closest to 0.0) is selected. The array of 1D lightrays that originate from the gridded viewplane result in a 2D image of the object(s) projected onto that viewplane.

Since the objects have been Lorentz transformed prior to the intersection, such that their geometry is correct for the camera frame in which the intersection occurs, the geometric components of the lighting model, the surface normal and the reflection angle, can be used to determine that pixel shade just as with a conventional lighting model in 3D rendering.

If the true pixel color is required, a relativistic Doppler shift must be applied to the color model at the surface intersection. This later step is not necessary to view the geometry of the object(s), and may in fact hider the object's visibility since, at relativistic velocities, light can Doppler shift out of the visible range.

4 RESULTS

It is critical that both the physical model as well as the visual representation are accurate and properly resolve relativistic optical properties. That is, if the 4D spacetime model is accurate, then it can be expected to manifest certain relativistic optical properties. Among these are motion, retarded time, Terrell rotation and relativistic aberration. Two characteristic classes of optical phenomena were examined and compared: low-speed effects and relativistic effects.

Low-speed effects are in this case, those for which the magnitude of the velocity vector of the object frame is less than 1% of the speed of light with respect to the camera frame: typically much less than 3,000 Km/sec. Those speeds encountered in day-to-day activities are in this category. A relativistic velocity of $0.866c$ was used for convenience, since at 86.6% of lightspeed the Lorentz factor is 2.0: objects contract to $\frac{1}{2}$ their rest length; and the object's time dilates to twice its proper time. In other words, the object's meter sticks are $\frac{1}{2}$ of a meter long as measured in the rest frame; and for each second that is ticked off by the object's clock, two seconds will pass in the rest frame.

The non-relativistic objects in this paper travel at $0.00866c$. In some cases, an instantaneous lightray was used (i.e. the lightspeed was set to infinity) to show by comparison, the effects of a finite lightspeed.

A visual software test fixture (VSTF) was created that would display animated sequences for user specifiable object shapes, positions and relativistic velocities, as well as camera position, attitude and velocity. The VSTF displays both 3D and 4D objects allowing visualized 4D objects to be compared to 3D test points visualized via conventional algorithms. The VSTF can operate in a debug mode, providing a means to interactively examine variables or to log results for later comparison against expected results.

For the following test cases, the unit of time is the tick of an arbitrary clock, and its spatial unit is the distance that light travels in one tick of this universal clock. As stated in Section 2.1, natural units will be used throughout such that the unit of measure for the spatial axes and the time axis is the *unit*. However, for pedagogical clarity the t axis or time units will be referred to by the term $t.unit$s and the spatial units will be referred to as $l.unit$s, but $t.unit \equiv l.unit$.

As shown in Figure 9 the VSTF displays a stage overlaid with a 12x12 grid. The red (darker shaded) grid lines with cross-section of $\frac{1}{20}$ of an $l.unit$, are on one $l.unit$ centers, as are the red (or darker shaded) rungs on the green (or lighter shaded) rails suspended four $l.unit$s above the stage. The green (or lighter shaded) grid lines represent the X and Z axes on the stage. The stage and these tickmarks as shown are identical for both non-relativistic and relativistic images. Light takes about 8.66 seconds to cross the stage. To give a sense of scale, this is equivalent to a 2.596 Million Km stage which could comfortably accommodate Jupiter and the orbit of it's moon, Ganymede. Each $l.unit$ is 216,350 Km, and a $t.unit$ is 0.721 seconds. The corresponding animations were rendered at 10 video-frames per $t.unit$ (except for the example in section 4.1.2) and are available online at [1].

4.1 Visual Evidence

Figures 9 - 18 demonstrate that our spacetime model accurately displays a 3D object moving at up to relativistic velocities and accurately renders the effects of retarded time, Terrell rotation, and aberration. The first two figures (Figures 9 & 10) demonstrate that for non-relativistic motion (e.g. $\beta = 0.00866$), the model yields the expected results.

4.1.1 Animation as a Property of Spacetime

Although not an emergent property[5], animation of a 3D object *emerges* as a result of the object's representation within this 4D spacetime model. Video-frames from the animation are shown in figures 9 and 10. These images were rendered by moving the camera from $(t,x,y,z)_{cam} = (940,0,6,15)$ for video-frame 920 to $(t,x,y,z)_{cam} = (1171,0,6,15)$ for video-frame 1151 (the camera was moved ahead 20 frames to allow enough time for the light to reach the camera). The accompanying animation sequences further demonstrate the emergence of animation from a *static* spacetime scene.

In these sequences, the simple right-angle flange has the following dimensions: 4.0 $l.unit$s high by 2.0 $l.unit$s wide by 2.0 $l.unit$s deep. The faces have no depth (being merely two-sided planes).

[5]Emergent properties arise out of more fundamental entities and yet are novel or irreducible with respect to them. [15]

The flange is constructed and temporally extruded as described in Section 3.1

4.1.2 Retarded Time

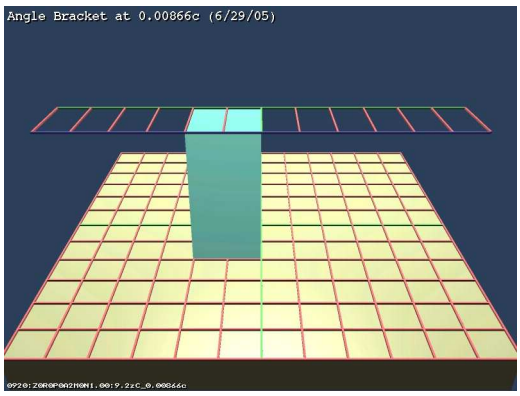

Figure 9: Right moving flange at $x = 0$ in video-frame 920.

In the first demonstration, the flange was encoded with a velocity of $0.00866c$ by offsetting the flange during the extrusion process as described in Section 3.1. A Δx of 17.32 $l.units$ for an elapsed time (Δt) of 2000 $t.units$ was coded, yielding

$$V_{exp} = \frac{\Delta x}{\Delta t} = \frac{17.32\ l.units}{2000\ t.units} = 0.00866 \frac{l.units}{t.unit}.$$

In Figure 9, the flange is moving from left to right at 0.866% of lightspeed. Using the crossing green lines on the stage as the origin, the camera is at $(0, 9, 15)$. Figure 9 shows the position of the moving flange with respect to the stage's grid marks within 0.05 $l.units$. Note that the flange lies exactly between $x = -2$ and $x = 0$.

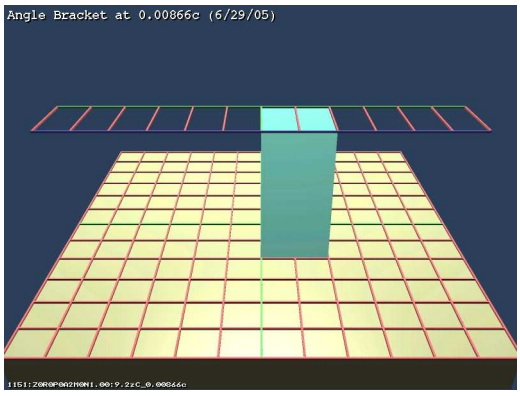

Figure 10: Right moving flange at $x = 2$ in video-frame 1151.

Examining Figure 9 and Figure 10 demonstrate that the algorithm is accurate. Figure 9 shows video-frame 920 with the right edge of the flange at the center gridline $x = 0$ of the stage. Figure 10 shows fame 1151 with the right edge of the flange at $x = 2$, giving a Δx of 2.0 ± 0.05 and a Δt of 231. At an animation rate of 1 $t.unit$ per video-frame, this yields a velocity of approximately

$$V = \frac{\Delta x}{\Delta t} = \frac{2}{231 * 1} \frac{l.units}{t.unit} = 0.00866 \frac{l.units}{t.unit} \pm 2.5\%.$$

By comparing Figure 9 at video-frame 920 with Figure 10 at vide-frame 1151 it can be seen that the image of the flange has moved 2.0 $l.units$ in 231 video-frames (231 $t.units$) or 0.008658 $\frac{l.units}{t.unit}$, within the expected value to better than 0.02% at non-relativistic speeds. The accuracy thus meets or exceeds the precision of the visual measurement procedure.

At the stated non-relativistic velocity, the relativistic effects are not visible. However, if the velocity is increased by 2 orders of magnitude, from $0.00866c$ to $0.866c$, then relativistic effects are observable, as is shown in the next section.

4.1.3 Classical Aberration

To demonstrate classic aberration, four depictions of the view of a distant object (star) were generated. The four positions on the Earth's orbit as shown in Figure 11 were chosen. These images are displayed below in Figures 13 and 15.

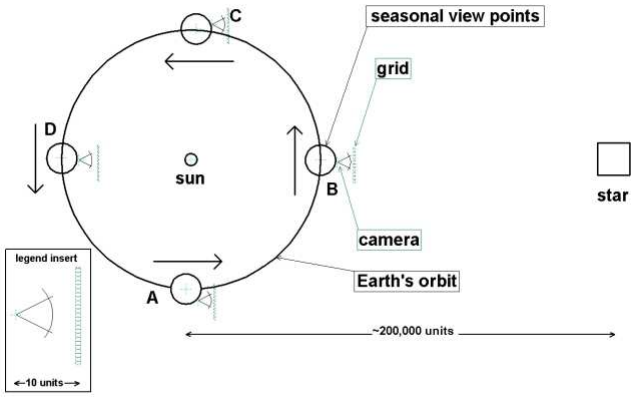

Figure 11: The four seasonal views from Earth
Earth's position in orbit with respect to star (cube) in Figures 13 and 15.
A) Top left - approaching; B) Top right - moving left;
C) Bottom left - receding; D) Bottom right - moving right;

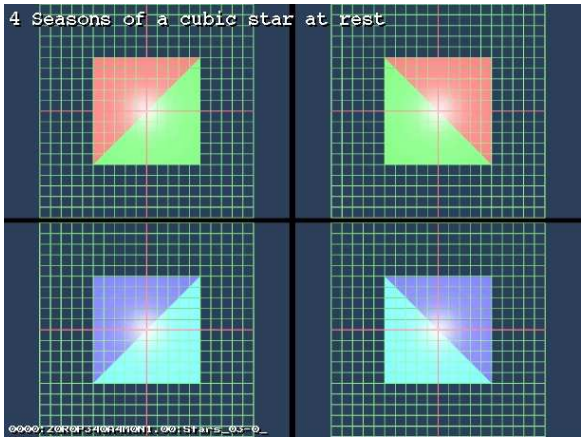

Figure 12: No Aberration - Observer at Rest
Control Frame to show image with observer at rest.

Figure 12 is a control-frame that depicts the cube (representing the star) from the four cardinal positions while at rest. Figure 13 shows the same four views of the cube, representative of the view of a star as seen from the Earth at three month intervals as it orbits about the sun. Note that the cubes project onto the center of the reference grid 10 unit sides, as shown in each view from the observer

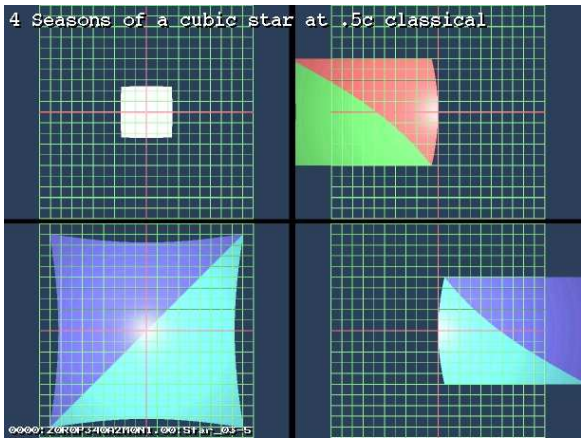

Figure 13: Classical Aberration Model
Seasonal views of a star from Earth (with orbital velocity of 0.5c)
Top left - Earth approaching; Top right - Earth moving left;
Bottom left - Earth receding; Bottom right - Earth moving right;

at rest. Figure 11 depicts and Figure 13 shows, clockwise from the top left: (top left) the Earth approaching the star and the star's area compressing; (top right) the Earth moving to the left and the star migrating to the front of the moving Earth; (bottom right) the Earth moving to the right and the star migrating to the right; and (bottom left) the Earth moving away from the star and the star's image expanding to envelope the visual sphere. The classical model will limit the aberration to less than 45 degrees, while the relativistic model in the next section, will allow the retreating star to envelope the entire visual sphere.

The cube is 1E5 units on a side, and lies 1.5E5 units from the observer (camera). The 20x20 grid lies between the cube and the observer 10 units from the observer. The cube and grid are positioned such that the cube (at rest) projects a 10x10 silhouette onto the grid centered on the red cross-hairs. So the cube at rest subtends an angle of arctan $\frac{10}{10}$ or 45° from the observer. Note that at 0.5c, the top right cube migrates approximately 26.6 degrees in the direction of motion of the observer with respect to the cube. This can be confirmed visually by noting that the right edge of the cube has move 5 grid marks left which equals arctan $\frac{5}{10} = 26.565°$.

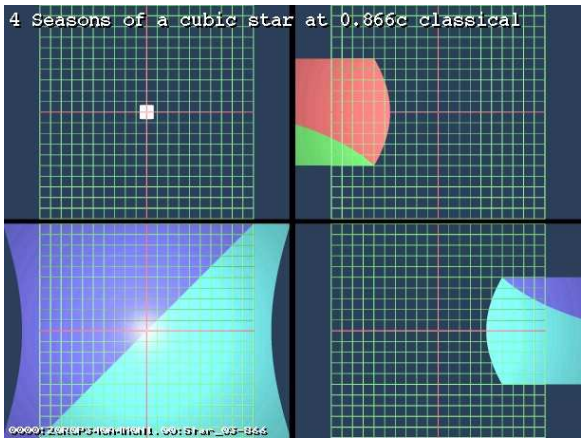

Figure 14: Classical Aberration Model at 0.866c

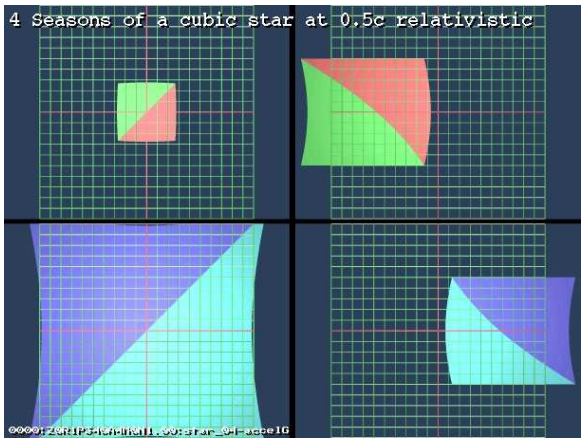

Figure 15: Relativistic Aberration Model
Seasonal views of a star from Earth (with orbital velocity of 0.5c)
Top left - Earth approaching; Top right - Earth moving left;
Bottom left - Earth receding; Bottom right - Earth moving right;

4.1.4 Relativistic Aberration

Relativistic aberration is likewise visualized with four views corresponding to views from four seasons of the Earth's orbit as depicted in Figure 11. The relativistic model introduces Lorentz length contraction of both the object, and the space in which the object is embedded. This leads to additional distortions in the object's geometry beyond those apparent for classical aberration, and will be obvious in the approach and retreat images.

Figure 15 shows four views of a cube, similar to that described in Section 4.1.3, Classical Aberration, above. As with the scene above, the cube at rest subtends an angle of arctan $\frac{10}{10}$ or 45° from the observer. Note that at 0.5c, the top right cube migrates approximately 30° in the direction of motion of the observer with respect to the cube, slightly greater than the 26.565° of the Classical model, above. This can be confirmed visually by noting that the right edge of the cube has moved 5.77 grid marks left which equals: arctan $\frac{5.77}{10} = 30.0°$.

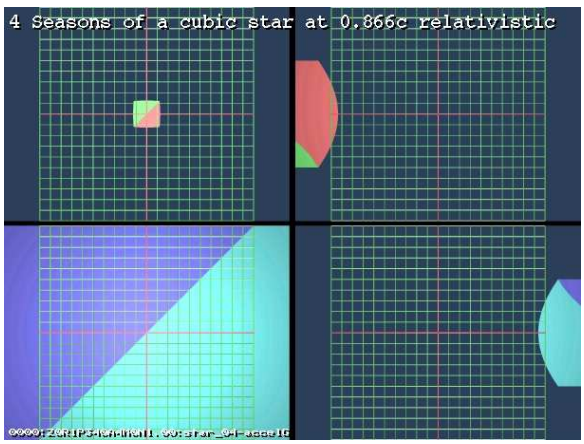

Figure 16: Relativistic Aberration Model at 0.866c

The relativistic contribution is obvious in the leftmost two panels of Figure 15 showing approaching and retreating objects. While in the classical model, the lightspeed limits the angular distortion in a retreating view of an object to 45°, the relativistic model's angular aberration of an object trailing the observer can reach nearly

180°. The result is that at 0.866*c*, the cube's edge moves from a position with respect to the direction of motion of 153.4° to 93.6°, effectively filling the panel, as shown in Figure 16 .

4.1.5 The Teaser Images

The finite lightspeed was decoupled from the physical effects in order to observe the respective contributions. The five teaser images (Figure 1) on the first page of this paper depict both decoupled finite lightspeed effects with no Lorentz transform and Lorentz transformed relativistic objects. The images depict the ubiquitous flange approaching, crossing, and departing the centerline of the scene at 0.866*c*. The top third of the image depicts an infinite lightspeed as per contemporary rendering, the middle third depicts a classical model of finite lightspeed with no physical effects, and the bottom third depicts the relativistic model showing the Lorentz contraction effects. The finite lightspeed camera was moved ahead in time (18.675 *t.unit*s), an amount equal to the lightspeed delay from the center of the stage to the camera, so that the flanges appear to be in approximately the same positions. The top view would be impossible to capture from any camera position or camera inertial reference frame without computer graphics[6].

Note that the bottom flanges *appear* to cross each other before the top flanges. Note also, that even with this head start, the top flanges arrive at their respective edges at the same time as the bottom flanges. The bottom flanges appear to approach faster and retreat slower than the top flanges. This is the visual evidence of the classical aberration effect. The flanges approaching the centerline of the stage are effectively approaching the camera, which is relativistically equivalent to the camera approaching each of the individual flanges. This configuration causes the angle from the centerline to the flanges to appear smaller than the proper angle of incidence, so the object appears closer to the centerline, or ahead of the object's proper position as depicted in the top view, and as predicted by Equation 1.

This is true for both the leading and the trailing edges of the flange, independently. As a result, the leading edge, which is closer to the centerline, has seemed to move further than the trailing edge, giving the impression of a wider flange. The opposite effect occurs as the flanges move away from the centerline. The flanges appear to incrementally speed up and simultaneously contract as they move relativistically away from the camera. These aberration effects are apparent in the bottom two images of Figure 1.

4.1.6 Terrell-Penrose-Boas Rotation

Terrell and Penrose predicted that an object moving past an observer relativistically, would appear to rotate in the direction of motion. This effect can be seen clearly in Figure 18, where the flange is moving from left to right at 0.866*c*. This is the same object, in the same position, as in Figure 17.

The classical distortion is an optical effect due to the finite limitation of the speed of light. The camera is at (0,9,15). As can be seen in Figure 17, when the flange's trailing edge is coincident with the $X = 0$ plane, the object's trailing upper left corner is at (0,4,2). This corner is then at a distance of [0,9,15] -[0,4,2] or 13.9 *l.unit*s from the camera. The trailing lower left corner is at (0,0,2), so the camera is at a distance of [0,9,15]-[0,0,2], or 15.8 *l.unit*s. Light will thus take 13.9 *t.unit*s to get to the camera from the first corner, and 15.8 *t.unit*s from the second corner, yielding a difference of 1.9 *t.unit*s. In 1.9 *t.unit*s, at 0.866c, the flange could travel 1.66 *l.unit*s, resulting in the trailing bottom edge of the flange being about 1.66 *l.unit*s behind the top trailing edge.

[6]In reality, without computer visualization, the top views could only be physically captured from three separate cameras in three separate inertial reference frames and then matted together.

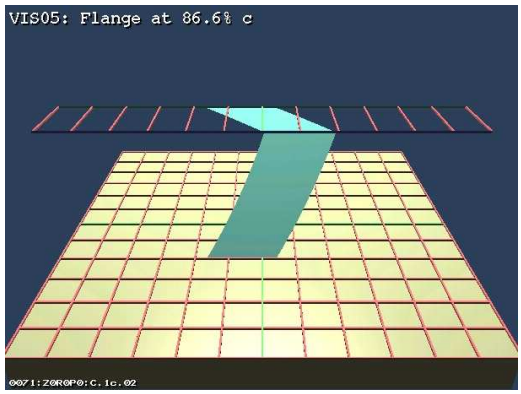

Figure 17: Terrell rotated flange (Lorentz decoupled)

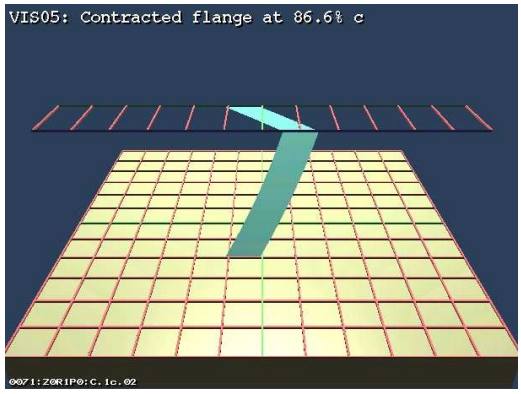

Figure 18: Terrell rotated and Lorentz contracted flange

Careful examination of Figure 18 shows this to be the case, the apparent distance of the lower left corner of the flange from the green $x = 0$ gridline is about 1.66 *l.unit*s. Similarly the furthest top edge of the flange appears to coincidentally be trailing by the same distance behind the closest top edge. The overhead red rungs, between the green rails, are likewise spaced one *l.unit* apart and can be used to reference the furthest top edge's trailing corner. This corner is at (0, 4, 0), and so is [0,9,15]-[0,4,0], or 15.8 *t.unit* from the camera, the same as the trailing bottom corner. This coincidence was arranged by suitable placement of the camera, and demonstrates that the algorithm implemented in the VSTF is visibly accurate to within at least two decimal places.

Boas [2] predicted that straight lines would appear curved. This effect can be seen in the vertical edges of the flange in Figure 17. In addition, the masking of the Lorentz contraction is depicted in Figure 18. This is the same view as Figure 17, but with Lorentz contraction restored. As can be seen, the flange has contracted to exactly $\frac{1}{2}$ its proper length. Note also that the Terrell rotation has filled in for the contraction, thus masking the Lorentz contraction as predicted by Terrell.

5 Conclusions

Applying the principles of special relativity has yielded animation sequences of 3D objects by 4D raytracing of static 3-manifolds embedded in a 4D spacetime without modifying the 3D scene between video-frames. The 3D objects were extruded into a 4th dimension orthogonal to the 3D axes. It was demonstrated that the apparent velocity of the animated object was related to the angle between the

extrusion and this 4th axis. A raytracing engine was developed to intersect its rays with these 4D objects from various points-of-view coincident with the 4th axis. It was demonstrated that if the point-of-view was advanced along this 4th axis, the objects appeared to move at velocities corresponding to the above described extrusion angle of the objects to this 4th axis. The objects exhibited characteristics attributed to objects moving with relativistic velocities with respect to the camera, such as Penrose-Terrell rotation, aberration and retarded position.

The Spacetime Raytracing strategy accurately renders objects with velocities from zero to the lightspeed-limit without modifying the object database between video-frames. The rendered image includes the usual photorealistic raytrace features such as reflection and shadows. Anti-aliasing can be extended into 4D to provide motion-blur. The non-relativistic optical effects of relativistic velocities are intrinsic properties of the algorithm and naturally emerge as the object velocity with respect to the observer approaches the speed of light. Similar techniques could be applied to exploring the geometric properties of extra dimensions.

ACKNOWLEDGEMENTS

Thanks to Dr James Arvo of the UCI Donald Bren School of Information and Computer Sciences for the ToyTracer raytrace kernel source code.

REFERENCES

[1] Don V. Black. Spacetime visualization videos. http://www.HyperVisualization.com/videos/black, 2004.

[2] Mary L. Boas. Apparent shape of large objects at relativistic speeds. *American Journal of Physics*, 29(5):283–286, May 1961.

[3] Max Born. *Einstein's Theory of Relativity*. Dover Publications, 1962.

[4] M. D'Zmura, P. Colantoni, and G. Seyranian. Virtual environments with four or more spatial dimensions. *Presence 9*, pages 616–631, 2001.

[5] Albert Einstein. On the electrodynamics of moving bodies. *Annalen der Physik*, (17), 1905.

[6] Albert Einstein. *Relativity, The Special and General Theory*. Pi Press, New York, 2005, 1916. Pi Press edition printed in 2005.

[7] Albert Einstein. *Relativity, The Special and General Theory*, chapter 16, Experience and the Special Theory of Relativity. Random House, Inc., New York, 1961, 1916.

[8] Albert Einstein. *Relativity, The Special and General Theory*, chapter Appendix 2, Minkowski's Four Dimensional Space ("World"). Random House, Inc., New York, 1961, 1916.

[9] Albert Einstein. *Relativity, The Special and General Theory*, chapter 17, Minkowski's Four Dimensional Space. Random House, Inc., New York, 1961, 1916.

[10] Andrew S. Glassner. Spacetime raytracing for animation. *IEEE Computer Graphics and Applications*, 8(2):60–70, March 1988.

[11] P.-K. Hsiung and R.H.P. Dunn. Visualizing relativistic effects in spacetime. In *Proceedings of Supercomputing '89 Conference*, pages 597–606, 1989.

[12] P.-K. Hsiung and R.H. Thibadeau. Time dilation visualization in relativity. In *Proceedings of Supercomputing*, pages 835–844. IEEE Computer Society, IEEE Computer Society Press, 1990.

[13] P.-K. Hsiung, R.H. Thibadeau, and M. Wu. T-buffer: Fast visualization of relativistic effects in spacetime. In *Symposium on Interactive 3D Graphics*, number 24 in 2, pages 83–88. SIGGRAPH, ACM, 1990.

[14] H.A. Lorentz, A. Einstein, H. Minkowski, and H. Weyl. *The Principle of Relativity*, chapter V: H. Minkowski. Space and Time. Cologne, 1908. Dover Publications, 1923.

[15] Timothy O'Connor and Hong Yu Wong. Emergent properties. In Edward N. Zalta, editor, *The Stanford Encyclopedia of Philosophy*. Stanford University, Summer 2005.

[16] Wolfgang Pauli. *Theory of Relativity*. Pergamon Press, 1958. Page 17, Eqn (13).

[17] Roger Penrose. The apparent shape of a relativistically moving sphere. In *Proceedings of Cambridge Philosophical Society*, number 55, pages 137–139, 1959.

[18] R. Rau, D. Weiskopf, and H. Ruder. Special relativity in virtual reality. In *International Workshop on Visualization and Mathematics*. VisMath, 1997.

[19] Wolfgang Rindler. *Introduction to Special Relativity, 2nd Ed*. Oxford Science Publications, 1982. Eqns (13.3) & (18.2).

[20] C. M. Savage and Antony C. Searle. Visualizing special relativity. http://www.anu.edu.au/Physics/Searle/, 1997. Dept. of Physics and Theoretical Physics, Australian National University.

[21] James Terrell. Invisibility of the lorentz contraction. *Physical Review*, 116(4):1041–1045, November 1959.

[22] D. Weiskopf, D. Kobras, and H. Ruder. Real-world relativity: Image-based special relativistic visualization. In *IEEE Visualization 2000 Proceedings*, pages 303–310. IEEE, 2001.

[23] Daniel Weiskopf. *Visualization of Four-Dimensional Spacetimes*. Ph.D. dissertation, University of Tübingen, 2001.